Check for updates

The Journal of Physiology

In vivo treatment with calcilytic of CaSR knock-in mice ameliorates renal phenotype reversing downregulation of the vasopressin-AQP2 pathway

Marianna Ranieri[1], Ines Angelini[1], Mariagrazia D'Agostino[1], Annarita Di Mise[1], Mariangela Centrone[1], Maria Venneri[2], Angela Ferrulli[1], Maria Mastrodonato[1], Grazia Tamma[1], Itsuro Endo[3], Seiji Fukumoto[4], Toshio Matsumoto[4] and Giovanna Valenti[1]

[1]*Department of Biosciences, Biotechnologies and Environment, University of Bari, Italy*
[2]*Istituti Clinici Scientifici Maugeri SPA SB IRCCS, Bari, Italy*
[3]*Department of Bioregulatory Sciences, Tokushima University, Tokushima, Japan*
[4]*Fujii Memorial Institute of Medical Sciences, Tokushima University, Tokushima, Japan*

Handling Editors: Kim Barrett & Robert Fenton

The peer review history is available in the Supporting Information section of this article (https://doi.org/10.1113/JP284233#support-information-section).

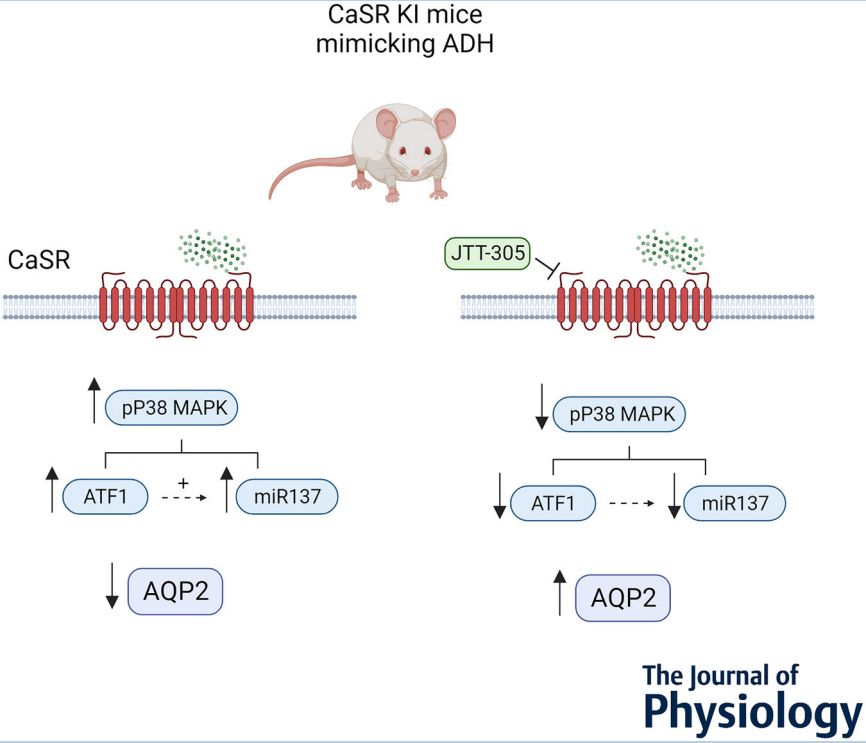

Abstract High concentrations of urinary calcium counteract vasopressin action via the activation of the Calcium-Sensing Receptor (CaSR) expressed in the luminal membrane of the collecting duct cells, which impairs the trafficking of aquaporin-2 (AQP2). In line with these findings, we provide evidence that, with respect to wild-type mice, CaSR knock-in (KI) mice mimicking autosomal dominant hypocalcaemia, display a significant decrease in the total content of AQP2 associated with significantly higher levels of AQP2 phosphorylation at Ser261, a phosphorylation site involved

This article forms part of the 'Aquaporins in Health and Disease' symposium held at Copenhagen in September 2022, and organised by Robert Fenton.

© 2024 The Authors. *The Journal of Physiology* © 2024 The Physiological Society. DOI: 10.1113/JP284233

in AQP2 degradation. Interestingly, KI mice also had significantly higher levels of phosphorylated p38MAPK, a downstream effector of CaSR and known to phosphorylate AQP2 at Ser261. Moreover, ATF1 phosphorylated at Ser63, a transcription factor downstream of p38MAPK, was significantly higher in KI. In addition, KI mice had significantly higher levels of AQP2-targeting miRNA137 consistent with a post-transcriptional downregulation of AQP2. *In vivo* treatment of KI mice with the calcilytic JTT-305, a CaSR antagonist, increased AQP2 expression and reduced AQP2-targeting miRNA137 levels in KI mice. Together, these results provide direct evidence for a critical role of CaSR in impairing both short-term vasopressin response by increasing AQP2-pS261, as well as AQP2 abundance, via the p38MAPK-ATF1-miR137 pathway.

(Received 17 October 2023; accepted after revision 30 January 2024; first published online 16 February 2024)
Corresponding author M. Ranieri: Department of Biosciences, Biotechnologies and Environment, University of Bari, Italy 70125. Email: marianna.ranieri@uniba.it and G. Valenti: Department of Biosciences, Biotechnologies and Environment, University of Bari, Italy 70125. Email: giovanna.valenti@uniba.it

Abstract figure legend Proposed model for signalling of activating mutation of Calcium-Sensing Receptor (CaSR) causing autosomal dominant hypocalcaemia (ADH), characterized by hypocalcaemia, hyperphosphatemia, and hypercalciuria. The activating mutation located in the transmembrane domain (A843E) generated a strain of CaSR knock-in mice used as an ADH mouse model. This CaSR gain-of-function mutation is associated with increased levels of p38MAPK which activates the transcriptor factor ATF1, which in turn may induce (dotted lines) the transcription of the miRNA137, a well-known aquaporin-2 (AQP2)-mRNA targeting microRNA, causing the reduction of AQP2 expression. The novel short-acting calcilytic, JTT-305 counteracts the p38MAPK-ATF1-miR137-AQP2 pathway, ameliorating the renal phenotype and representing a possible new therapeutic agent to reverse most of the anomalies in calcium metabolism in ADH patients caused by activating mutations of CaSR.

Key points

- Calcium-Sensing Receptor (CaSR) activating mutations are the main cause of autosomal dominant hypocalcaemia (ADH) characterized by inappropriate renal calcium excretion leading to hypocalcaemia and hypercalciuria. Current treatments of ADH patients with parathyroid hormone, although improving hypocalcaemia, do not improve hypercalciuria or nephrocalcinosis.
- *In vivo* treatment with calcilytic JTT-305/MK-5442 ameliorates most of the ADH phenotypes of the CaSR knock-in mice including hypercalciuria or nephrocalcinosis and reverses the down-regulation of the vasopressin-sensitive aquaporin-2 (AQP2) expression, providing direct evidence for a critical role of CaSR in impairing vasopressin response.
- The beneficial effect of calcilytic in reducing the risk of renal calcification may occur in a parathyroid hormone-independent action through vasopressin-dependent inhibition of cAMP synthesis in the thick ascending limb and in the collecting duct.
- The amelioration of most of the abnormalities in calcium metabolism including hypercalciuria, renal calcification, and AQP2-mediated osmotic water reabsorption makes calcilytic a good candidate as a novel therapeutic agent for ADH.

Marianna Ranieri obtained her PhD in 'Cellular and Molecular Technologies in Physiology' in 2007, at the University of Bari, Italy. Next, she achieved a Postdoctoral Research Fellowship within an international FIRB grant. Currently, she is Assistant professor in the Department of Biosciences, Biotechnology and Environment. Her research is focused on the signal transduction of the extracellular Calcium Sensing Receptor and its pathophysiological role in hypertension and kidney disorders. She has focused my studies on the functional interaction of CaSR with renal aquaporins both *in vitro* and *in vivo* models, demonstrating a negative feedback from CaSR signalling to V2R/AQP2 pathway in regulating water reabsorption.

© 2024 The Authors. *The Journal of Physiology* © 2024 The Physiological Society.

14697793, 0, Downloaded from https://physoc.onlinelibrary.wiley.com/doi/10.1113/JP284233 by University Degli Studi Di Bari, Wiley Online Library on [27/02/2024]. See the Terms and Conditions (https://onlinelibrary.wiley.com/terms-and-conditions) on Wiley Online Library for rules of use; OA articles are governed by the applicable Creative Commons License

Introduction

Calcium-Sensing Receptor (CaSR) is a seven-transmembrane (7TM) domain receptor coupled to G-proteins and belonging to the C family, characterized by a large extracellular domain composed of a Venus Flytrap (VFT) domain where agonists bind, linked to the 7TM domain via a cysteine-rich rigid segment. CaSR is a mandatory dimer in which the monomers are associated via the N-terminal lobe of the VFT.

In the kidney, CaSR is expressed in all segments (Riccardi & Valenti, 2016), showing major expression on the basolateral membrane of the thick ascending limb (TAL). In TAL, CaSR plays a crucial role in the regulation of mineral cation transport inhibiting calcium reabsorption in response to increased plasma calcium levels (Brown & MacLeod, 2001; Hebert et al., 1997; Pearce & Thakker, 1997; Ward & Riccardi, 2002).

CaSR is also expressed on the apical membrane of the proximal tubule cells, where it directly blunts the phosphaturic action on the parathyroid hormone (PTH), modulating the inhibitory action of PTH on Pi absorption (Ba et al., 2003).

In the distal tubule, CaSR is co-expressed with the vacuolar H^+-ATPase at the apical membrane of the inter-calated cells of the collecting duct, while on the apical membrane of the principal cells, CaSR is co-expressed with aquaporin-2 (AQP2) (Sands et al., 1997). Here, the CaSR senses urinary Ca^{2+} and regulates water reabsorption to control hypercalciuria and prevent Ca^{2+} precipitation (Vezzoli et al., 2011). These two important signalling activated by CaSR together result in the production of dilute, acidified urine, which reduces the risk of nephrolithiasis (Nedvetsky et al., 2009; Ranieri et al., 2015).

CaSR inactivating mutations cause neonatal severe hyperparathyroidism (NSHPT, OMIM# 239 200) and familial hypocalciuric hypercalcaemia (FHH, OMIM# 145 980), also known as familial benign hypercalcaemia (Pollak et al., 1993). Conversely, activating mutations are the main causes of autosomal dominant hypocalcaemia (ADH, OMIM# 146 200), described as hypocalcaemia, hyperphosphatemic and hypercalciuric disorder (Pollak et al., 1994).

Inherited or *de novo* activating variants of the CASR alter the sensitivity of cells to the extracellular calcium, resulting in inadequate PTH secretion and inappropriate renal calcium excretion, leading to hypocalcaemia and hypercalciuria. The conventional therapy includes calcium and vitamin D, which can worsen hypercalciuria, resulting in renal complications (Roszko, Stapleton Smith et al., 2022). Indeed, treatment of hypoparathyroidism with PTH ameliorates bone turnover (Sikjaer et al., 2011), increasing the amount of loss mineralized bone and the porosity of cortical bone (Gafni et al., 2012). By contrast, several studies showed that daily injection of PTH in ADH patients, although improving hypocalcaemia, did not improve hypercalciuria or nephrocalcinosis (Theman et al., 2009). The currently available treatments frequently cause considerable complications such as nephrolithiasis and renal impairment, prompting the demand for a new therapeutic approach to correct the hypersensitivity of mutated CaSR to serum Ca^{2+} in ADH patients.

Recently, we demonstrated that CaSR activation results in p38MAPK activation, which in turn phosphorylates transcription factors able to increase the gene transcription of microRNA miRNA137 (Ranieri, 2019; Ranieri et al., 2018). In the renal collecting duct, this miRNA is known as AQP2-targeting miRNA (Kim et al., 2015). CaSR-dependent activation of miRNA137 expression contributes to counteract the AQP2 expression and trafficking.

The present study aimed to investigate the functional interaction of the CaSR signalling and the vasopressin-AQP2 axis *in vivo* in CaSR knock-in (KI) mice harbouring activating mutations in the CASR gene. This animal model exhibited low bone turnover because of the deficiency of PTH, mimicking ADH (Dong et al., 2015). More specifically, the experimental strategy was to evaluate the effect of high-affinity CaSR antagonists, the calcilytics (Alfadda et al., 2014), on the vasopressin-AQP2 axis. Calcilytics are able to bind CaSR directly at transmembrane domain level (Petrel et al., 2004) and allosterically stimulate the endogenous release of PTH (Kumar et al., 2010). Several calcilytics have been used to decrease CaSR sensitivity to extracellular Ca^{2+}. In the present study, CaSR KI mice were treated with JTT-305 (also known as MK-5442), a short-acting calcilytic, already known to transiently enhance the endogenous PTH secretion and to increase bone mineral density (BMD) in rats (Kimura et al., 2011). Of note, the obtained results revealed that JTT-305 reversed the downregulation of the vasopressin-AQP2 pathway, thus ameliorating the CaSR KI ADH phenotype.

Methods

Ethical approval

All animal experimental procedures were performed in accordance with the guidelines of the Animal Research Committee of Tokushima University (T2020-109). This study was approved by the Genetic Modification Experiment Safety Management Committee of Tokushima University (2023-136).

Animal models

As ADH1 model mice, A843E mutant CaSR KI mice (Accession No. CDB1054K; http://www2.clst.riken.jp/arg/mutant%20mice%20list.html) were generated as described (http://www2.clst.riken.jp/arg/Methods.html).

© 2024 The Authors. *The Journal of Physiology* © 2024 The Physiological Society.

14697793, 0, Downloaded from https://physoc.onlinelibrary.wiley.com/doi/10.1113/JP284233 by University Degli Studi Di Bari, Wiley Online Library on [27/02/2024]. See the Terms and Conditions (https://onlinelibrary.wiley.com/terms-and-conditions) on Wiley Online Library for rules of use; OA articles are governed by the applicable Creative Commons License

Mice were housed under a 12:12 h light/dark photocycle (lights on 07.00 h) at 25°C, with free access to water and diet during the night cycle, and fed with diet containing 1.2% calcium, 0.8% phosphorus and 400 IU 100 g^{-1} vitamin D [Hough, 2004 #71] after weaning.

JTT-305/MK-5442 or vehicle (0.5 w/v% methylcellulose) was administered to mice by gastric gavage. No adverse events were observed within the doses of JTT-305/MK-5442 used in this study (2–50 mg g^{-1} body weight). Genotyping analysis of mice was performed by PCR analysis to detect both human CaSR and mouse CaSR using genomic DNA extracted from the tail as described previously (Dong et al., 2015). Mice were anaesthetized using isoflurane and killed by cervical dislocation at the time of kidney extraction. Three genotype mice [wild-type (WT), KI and KI+JTT-305], comprising three males and three females for each genotype, were used for all experiments.

Chemicals and reagents

All chemicals were purchased from Sigma-Aldrich (St Louis, MO, USA). Calcilytic JTT-305 (also known as MK-5442) was kindly provided by Japan Tobacco Inc. (Tokyo, Japan) and it was administered to mice by gastric gavage. SB203580 (p38MAPK inhibitor) was obtained from Cell Signalling Technology Inc. (Danvers, MA, USA). The miRNA assay and kit were purchased from Applied Biosystems (Foster City, CA, USA).

Antibodies

Mouse monoclonal antibody against AQP2-E2 (catalogue no. sc-515 770, lot no. J0820) was purchased from Santa Cruz Biotechnology (Tebu Bio, Milan, Italy). AQP2 polyphosphorylated region (CLKGLEPDTDWEEREVRRRQ) was used to detect the total amount of AQP2. AQP2-pS261 antibody was from Novus Biologicals (Littleton, CO, USA). p38MAPK, Pp38MAPK (Thr180/Tyr182) and ubiquitin (P4D1) antibodies were purchased from Cell Signalling Technology. Total ATF-1 and P-ATF-1 (Ser63) antibodies were from Santa Cruz Biotechnology. Secondary goat anti-rabbit (catalogue no. A0545, lot no. 083M4752) or anti-mouse (catalogue no. A9044, lot no. 055M4818) horseradish peroxidase-coupled antibodies were obtained from Santa Cruz Biotechnology. Secondary goat anti-rabbit Alexa555 conjugate antibodies was from Molecular Probes (Eugene, OR, USA).

Kidney slices from mouse kidneys

The three genotype mice (WT, KI, and KI+JTT-305), three males and three females for each genotype, were anaesthetized and killed by cervical dislocation. Kidneys were quickly removed and 500 μm sections were made with a McIlwain tissue chopper. Kidney sections were equilibrated for 10 min at 37°C in buffer for kidney slices, containing 118 mM NaCl, 16 mMHepes, 17 mM Na-HEPES, 14 mM glucose, 3.2 mM KCl, 2.5 mM $CaCl_2$, 1.8 mM $MgSO_4$ and 1.8 mM KH_2PO_4 (pH 7.4), integrated with protease (1 mM phenylmethylsulfonyl fluoride, 2 mg mL^{-1} leupeptin and pepstatin A) and phosphatase inhibitors (10 mM NaF and 1 mM sodium orthovanadate). To test the role of p38MAPK, the kidney slices were incubated with the p38-MAPK inhibitor, SB203580, at 10 μM for 30 min at 37°C. Afterwards, treated sections were homogenized through a mini potter on ice-cold kidney slices buffer implemented with the previously mentioned inhibitors. Suspensions were finally centrifuged at 12 000 ***g*** for 10 min at 4°C and the supernatants were employed in western blot analysis or gene expression experiments.

Ubiquitination assay

After treatments, kidney slices were lysed into the immunoprecipitation buffer (150 mM 1% Triton X-100, 150 mM NaCl and 25 mM Hepes, pH 7.4, with 20 mM *N*-ethylmaleimide to block de-ubiquitination), in the presence of protease and phosphatase inhibitors. Lysates were clarified by centrifugation at 12 000 ***g*** for 10 min at 4°C. The obtained supernatants were precleared with protein A–sepharose suspension for 30 min under rotation at 4°C. The protein A-sepharose was previously hydrated into the immunoprecipitation buffer and incubated with the anti-AQP2 antibody under rotation at 4°C overnight. The next day, the immunocomplexes were washed three times, resuspended in Laemmli's buffer in non-denaturing conditions, and used for the immunoblotting analysis with anti-AQP2 and anti-ubiquitin antibodies.

Gel electrophoresis and western blotting

Proteins were separated using 12% stain-free polyacrylamide gels (Bio-Rad Laboratories, Inc., Hercules, CA, USA) under reducing conditions or 10% stain-free polyacrylamide gels (Bio-Rad Laboratories, Inc.) under non-denaturing conditions for ubiquitination experiments. Protein bands were electrophoretically transferred on polyvinylidene fluoride (PVDF) membranes (Thermo Fisher Scientific, Waltham, MA, USA) using the Trans-Blot Turbo Transfer System for the western blot analysis, blocked in Tris-buffered saline-Tween-20 containing 3% bovine serum albumin (BSA) and incubated with primary antibody overnight. Immunoreactive bands were detected with horseradish peroxidase-conjugated secondary antibody (Santa Cruz Biotechnology). Membranes were developed by using

© 2024 The Authors. *The Journal of Physiology* © 2024 The Physiological Society.

14697793, 0, Downloaded from https://physoc.onlinelibrary.wiley.com/doi/10.1113/JP284233 by University Degli Studi Di Bari, Wiley Online Library on [27/02/2024]. See the Terms and Conditions (https://onlinelibrary.wiley.com/terms-and-conditions) on Wiley Online Library for rules of use; OA articles are governed by the applicable Creative Commons License

Clarity Western ECL Blotting Substrate with a Chemidoc System (Bio-Rad Laboratories). The obtained bands were normalized to total protein using the stain-free technology gels. Densitometry was performed using Image Lab software (Bio-Rad Laboratories), displaying the optical density (O.D.) values.

Immunolocalization of AQP2 and AQP2-pS261 in kidney slices

For AQP2 immunolocalization, kidneys of each genotype (WT, KI, and KI+JTT-305) were embedded into paraffin blocks. Tissues were fixed by immersion in 4% paraformaldehyde in phosphate-buffered saline (PBS) at 4°C overnight; then, they were dehydrated and embedded into paraffin wax. The solidified paraffin blocks were trimmed and cut at 5 μm, and then the sections were separated from the paraffin ribbon and mounted onto slides. Afterwards, deparaffinization with histolemon was performed and the sections were hydrated through a graded series of ethanol (100%, 95%, 80%, 70%, and 50% ethanol) and distilled water. Hereafter, the sections were rinsed in PBS 1X several times before using them for immunostaining. Sections were exposed to permeabilization procedure with Triton X-100 0.01% and SDS 0.1% for 5 min. After washing in PBS, non-specific binding sites were blocked with 1% BSA in PBS (saturation buffer) for 45 min in a humidified chamber. Sections were incubated by drop with primary antibodies: mouse anti-AQP2 (dilution 1:1000) in 1% BSA in PBS for 1 h at room temperature, then overnight at 4°C. After washing five times in PBS, sections were incubated with the donkey anti-mouse Alexa Fluor 555 conjugated secondary antibody (dilution 1:1000) for 1 h and 30 min at room temperature. After more washes in PBS, sections were mounted on glass slides using Mowiol (Sigma-Aldrich) as mounting medium overnight at room temperature. Images were obtained with a confocal laser-scanning fluorescence microscope (TCS SP2; Leica Microsystems, Mannheim, Germany).

Real-time PCR analysis of AQP2 and activating transcription factor 1 (ATF-1) mRNA levels

Real-time PCR (RT-PCR) experiments were performed to measure the relative expression of mRNA in inner medulla collecting duct (IMCD) isolated from WT and KI mice kidneys. Total RNA was extracted using Trizol Reagent (Thermo Fisher Scientific). Complementary DNA (cDNA) was synthesized using Super Script Vilo Master Mix (Thermo Fisher Scientific), performing the reverse transcription on 1 μg of total RNA. RT-PCR amplification was performed using TaqMan Gene Expression Master Mix (Thermo Fisher Scientific). The real-time PCR mixture contained 10 μL of 2 × TaqMan, 8 μL of DNase and RNase free water, 1 μL of AQP2 or ATF-1 or 18S (endogenous control) assay, and 1 μL of cDNA sample. Assays were performed using a StepOne Real-Time PCR System (Applied Biosystems, Inc., Foster City, CA, USA). Amplification including one stage of 20 min at 95°C, followed by 40 cycles of a two-step loop: 1 s at 95°C and 20 s at 60°C. The comparative C_t ($\Delta\Delta C_t$) method was used to determine the relative target quantity in samples by comparing normalized target quantity in each sample to the normalized target quantity in the reference sample. The results were expressed as $2^{-\Delta\Delta C_t}$ values, with $\Delta\Delta C_t = (C_{t\ target} - C_{t\ 18S})_{KI} - (C_{t\ target} - C_{t\ 18S})_{WT}$.

miR137 evaluation

miR137 content in WT and KI mice IMCD was evaluated using a TaqMan Advanced miRNA Assay (has-miR-137; Assay ID: 477 904_mir; Applied Biosystems), which allows highly sensitive and specific amplification and quantification of mature miRNA through a quantitative PCR.

After the total RNA extraction using Trizol, the cDNA templates were obtained: the poly(A) tailing reaction, the adaptor ligation reaction, the RT-reaction, and the miR-Amp reaction were performed. To estimate the quantity (ng) of miR137 content in samples, a synthetic RNA (UUAUUGCUUAAGAAUACGCGUAG), synthesized by Applied Biosystems, was employed to create a calibration curve to interpolate miRNA samples values from WT, KI and KI mice treated with JTT-305. Next, the quantitative PCR amplification was performed.

Statistical analysis

All of the data are presented as the mean ± SD. Statistical differences are analysed either by an unpaired Student's *t* test between two groups or one-way analysis of variance followed by an appropriate (Tukey's) *post hoc* test for multiple comparisons. $P < 0.05$ was considered statistically significant.

Results

Reduced expression of AQP2 in the kidney of CaSR KI mice

First, we evaluated protein expression levels of AQP2 through immunoblotting experiments in kidneys obtained from WT and CaSR KI mice, using antibodies against AQP2 (Fig. 1*A*). AQP2 immunoreactive bands were normalized to total protein content and densitometric analysis revealed a robust reduction (more than 50%) in AQP2 levels in KI mice with respect

© 2024 The Authors. *The Journal of Physiology* © 2024 The Physiological Society.

14697793, 0, Downloaded from https://physoc.onlinelibrary.wiley.com/doi/10.1113/JP284233 by University Degli Studi Di Bari, Wiley Online Library on [27/02/2024]. See the Terms and Conditions (https://onlinelibrary.wiley.com/terms-and-conditions) on Wiley Online Library for rules of use; OA articles are governed by the applicable Creative Commons License

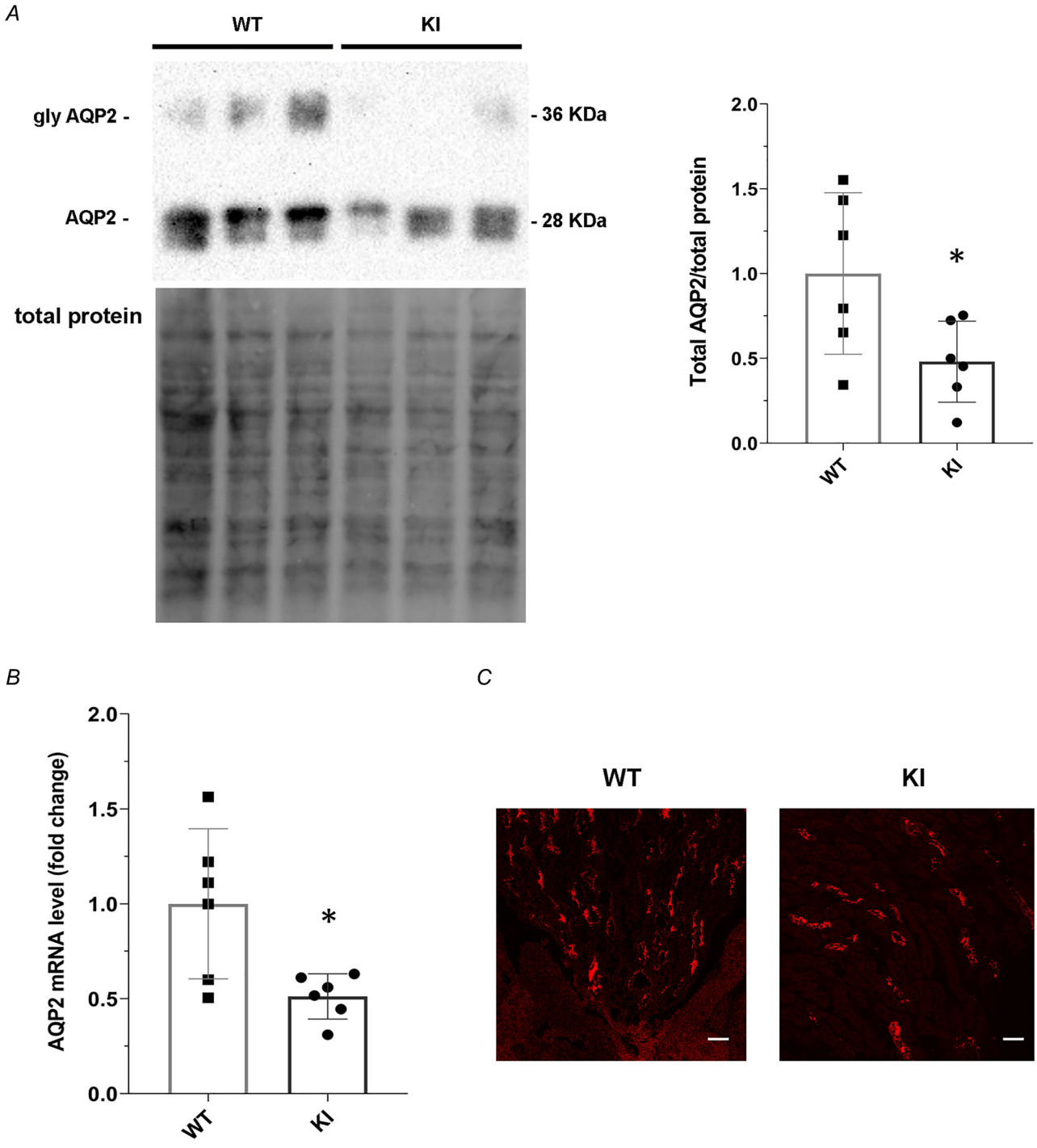

Figure 1. AQP2 expression and localization in the kidney from WT and KI mice
A, kidney slices from WT and KI mice were lysed and immunoblotting experiments were performed using specific antibodies against total AQP2. Densitometric analysis of total AQP2 bands normalized to the total protein content is reported in the histogram. Data are expressed as the mean ± SD (*P = 0.038 *vs*. WT). *B*, for the analysis of AQP2 mRNA levels, RNA was extracted from WT and KI mice kidneys as described in the Methods. Data are expressed as the mean ± SD (*P = 0.016 *vs*. WT). *C*, immunolocalization of AQP2 (in red) in the renal inner medulla from WT and KI mice. Reduced AQP2 immunofluorescence signal was observed in KI mice compared to WT (scale bar = 20 μm).

© 2024 The Authors. *The Journal of Physiology* © 2024 The Physiological Society.

14697793, 0, Downloaded from https://physoc.onlinelibrary.wiley.com/doi/10.1113/JP284233 by University Degli Studi Di Bari, Wiley Online Library on [27/02/2024]. See the Terms and Conditions (https://onlinelibrary.wiley.com/terms-and-conditions) on Wiley Online Library for rules of use; OA articles are governed by the applicable Creative Commons License

to WT mice [KI: 0.481 (0.239) *vs.* WT: 1.000 (0.477) O.D.; $P = 0.038$; $n = 6$ for each genotype] (Fig. 1*A*). Furthermore, evaluation of AQP2 mRNA extracted from WT and KI mouse kidneys and processed for RT-PCR (Fig. 1*B*) showed a significant reduction in AQP2 gene expression in KI compared to WT mice [KI: 0.512 (0.119) *vs.* WT: 1.000 (0.396); $P = 0.016$; $n = 6$ for each genotype] (Fig. 1*B*). According to the immunoblotting findings, immunolocalization and visualization by confocal microscopy validated a reduced expression of AQP2 in KI mice kidneys with respect to WT (Fig. 1*C*).

Effect of JTT-305 on AQP2 expression in the CaSR KI mice kidneys

The short-acting calcilytic JTT-305 or vehicle was administered to CaSR KI mice by gastric gavage. Therefore, we performed immunoblotting experiments to evaluate the expression of AQP2 at the protein level in kidneys obtained from CaSR KI mice treated with JTT-305 or with the vehicle only (Fig. 2*A*). AQP2 immunoreactive bands were normalized to total protein content and densitometric analysis revealed a significant and strong increase (∼2-fold) in AQP2 levels in KI mice treated with JTT-305 with respect to KI mice [KI+JTT-305: 2.878 (0.440) *vs.* KI: 1.000 (0.547) O.D.; $P = 0.000064$; $n = 6$ for each genotype] (Fig. 2*A*). Moreover, an evaluation of AQP2 mRNA extracted from KI and KI+JTT-305 mice kidneys was performed (Fig. 2*B*). The RT-PCR results revealed a significant increase in AQP2 gene expression in KI+JTT-305 mice compared to KI mice [KI+JTT-305: 1.959 (0.707) *vs.* KI: 1.000 (0.230); $P = 0.01$; $n = 6$ for each genotype] (Fig. 2*B*). Confocal microscopy immunolocalization and visualization confirmed the increased expression of AQP2 observed in KI+JTT-305 mice kidneys with respect to KI treated with the vehicle only (Fig. 2*C*). These findings clearly confirm the direct involvement of CaSR in the regulation of AQP2 gene and protein expression levels, as recently demonstrated (Ranieri et al., 2018).

Decreased AQP2 expression in the kidney of CaSR KI mice is correlated to the higher expression of AQP2-pS261, phosphorylated p38MAPK and polyubiquitinated AQP2: role of JTT-305

AQP2 function and expression are fine regulated by several post-translational modifications, such as phosphorylation, ubiquitination and degradation (Centrone et al., 2017; Moeller et al., 2011), and glutathionylation (Tamma, Ranieri et al., 2014). In the short term, vasopressin stimulation causes AQP2 phosphorylation in serine 256, 264 and 269; in the long term, AQP2 mRNA expression increases and, consequently, causes a rise in AQP2 protein level (Fenton & Moeller, 2008; Hoffert et al., 2008; Matsumura et al., 1997). On the other hand, phosphorylation at Ser261 of AQP2 is known to decrease under vasopressin stimulation (Hoffert et al., 2006, 2007; Matsumura et al., 1997; Nedvetsky et al., 2010). AQP2 phosphorylation at Ser261 and polyubiquitination by p38MAPK have been shown to induce AQP2 degradation (Nedvetsky et al., 2010; Trepiccione et al., 2014).

Considering the strong reduction in the AQP2 expression, we next evaluated whether the reduced AQP2 levels found in KI mice were accompanied by an increase in AQP2 phosphorylation at Ser261 (AQP2-pS261). Hence, we performed immunoblotting experiments in kidneys obtained from WT mice, CaSR KI mice and CaSR KI mice treated with JTT-305 (Fig. 3*A*). AQP2 immunoreactive bands were normalized to total protein content and total AQP2 levels, and densitometric analysis revealed a robust increase (78%) in AQP2-pS261 expression in KI mice compared to WT mice [KI: 1.780 (0.454) *vs.* WT: 1.000 (0.185) O.D.; $P = 0.0013$; $n = 6$ for each genotype] (Fig. 3*A*). Moreover, we analysed the AQP2-pS261 levels in CaSR KI mice treated with JTT-305. Compared with CaSR KI mice, the calcilytic treatment was able to significantly reduce the increased phosphorylation in Ser261 of AQP2 observed in CaSR KI mice treated with the vehicle only [KI+JTT-305: 0.549 (0.169) *vs.* KI: 1.780 (0.454) O.D.; $P = 0.00001$; $n = 6$ for each genotype] (Fig. 3*A*). Noteworthy, the JTT-305 treatment induced significantly lower AQP2-pS261 levels than that detectable in the WT mice ($P = 0.04$) (Fig. 3*A*). Because the expression of total AQP2 was significantly reduced in KI mice, post-translational modification related to an increase in cell surface expression of AQP2 namely the pS256-AQP2 and the pS269-AQP2 were not evaluated.

Ubiquitination is a mechanism aimed at targeting proteins intended for degradation (Li & Ye, 2008). A pioneering biochemical study showed that a single polyubiquitin chain is sufficient to target a model substrate to 26S proteasomes (Chau et al., 1989) and to be the principal proteasome delivery signal (Finley et al., 1994). Subsequently, it has become clear that mono- and polyubiquitin chains generally signal different fates for their target proteins (Sadowski et al., 2012): monoubiquitination leads to altered trafficking in multiple pathways (Hicke & Dunn, 2003), whereas polyubiquitin chains usually signal proteasome proteolysis (or degradation) (Flick et al., 2004; Thrower et al., 2000).

The analysis of ubiquitinated AQP2 by immunoblotting experiments revealed that, compared with WT mice, the levels of polyubiquitinated AQP2 normalized to immunoprecipitated AQP2 were more than 2-fold higher in kidneys from CaSR KI mice [KI: 2.229 (0.798) *vs.* WT: 1.000 (0.480) O.D.; $P = 0.004$; $n = 6$ for each genotype] (Fig. 3*B*). Of note, treatment with JTT-305

© 2024 The Authors. *The Journal of Physiology* © 2024 The Physiological Society.

14697793, 0, Downloaded from https://physoc.onlinelibrary.wiley.com/doi/10.1113/JP284233 by University Degli Studi Di Bari, Wiley Online Library on [27/02/2024]. See the Terms and Conditions (https://onlinelibrary.wiley.com/terms-and-conditions) on Wiley Online Library for rules of use; OA articles are governed by the applicable Creative Commons License

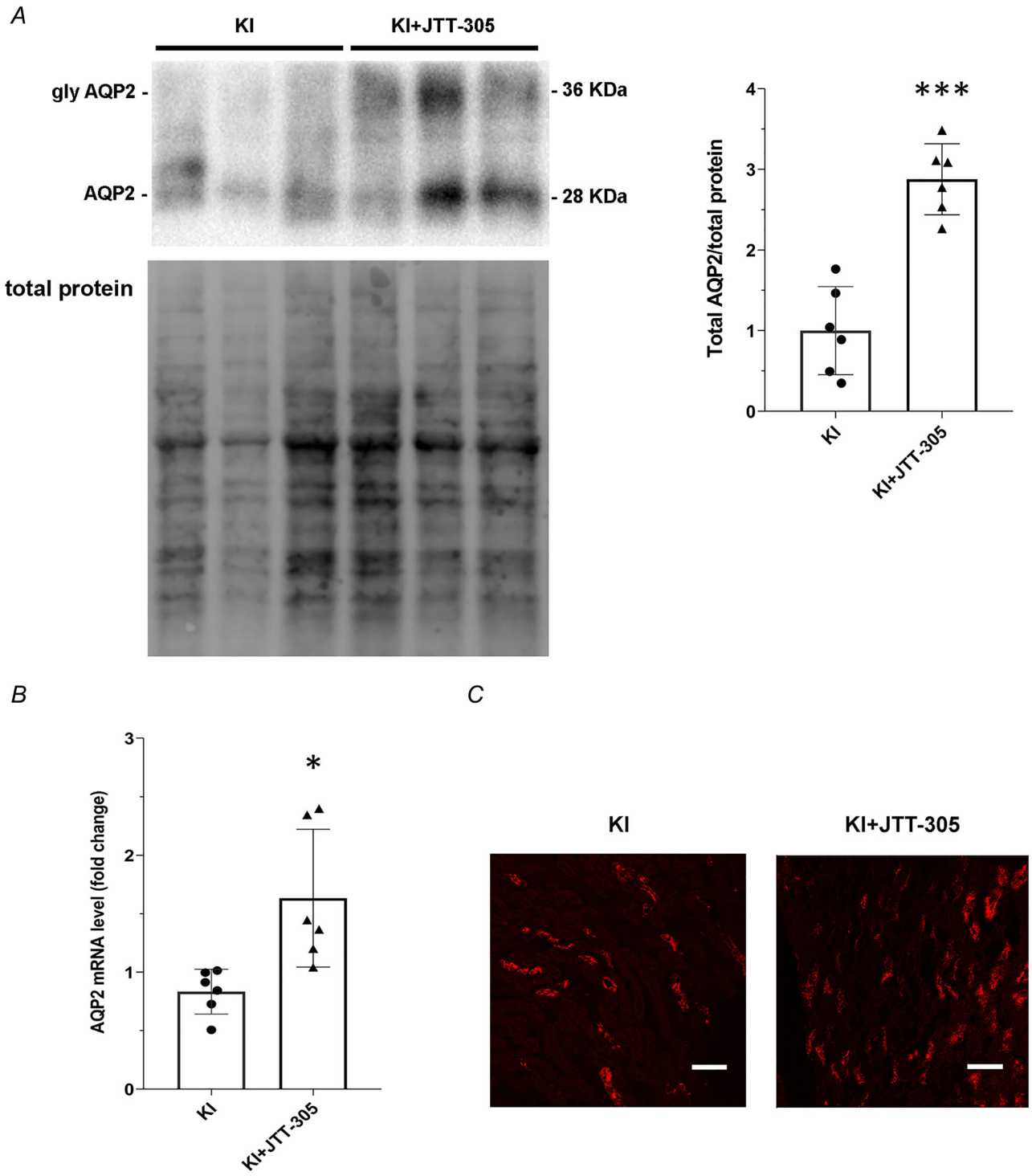

Figure 2. AQP2 expression and localization in the kidney from KI and JTT-305 treated KI mice
A, kidney slices from KI mice and KI mice treated with JTT-305 were lysed and immunoblotting experiments were performed using specific antibodies against total AQP2. Densitometric analysis of total AQP2 bands normalized to the total protein content is reported in the histogram. Data are expressed as the mean ± SD (***P = 0.000064 *vs.* KI). *B*, for the analysis of AQP2 mRNA levels, RNA was extracted from KI and JTT-305 treated KI mice kidneys as described in the Methods. Data are expressed as the mean ± SD (*P = 0.01 *vs.*KI). *C*, immunolocalization of AQP2 (in red) in the renal inner medulla from KI and JTT-305 treated KI mice. A higher AQP2 immunofluorescence signal was observed in KI treated with JTT-305 compared to KI mice kidney section (scale bar = 20 μm).

© 2024 The Authors. *The Journal of Physiology* © 2024 The Physiological Society.

14697793, 0, Downloaded from https://physoc.onlinelibrary.wiley.com/doi/10.1113/JP284233 by University Degli Studi Di Bari, Wiley Online Library on [27/02/2024]. See the Terms and Conditions (https://onlinelibrary.wiley.com/terms-and-conditions) on Wiley Online Library for rules of use; OA articles are governed by the applicable Creative Commons License

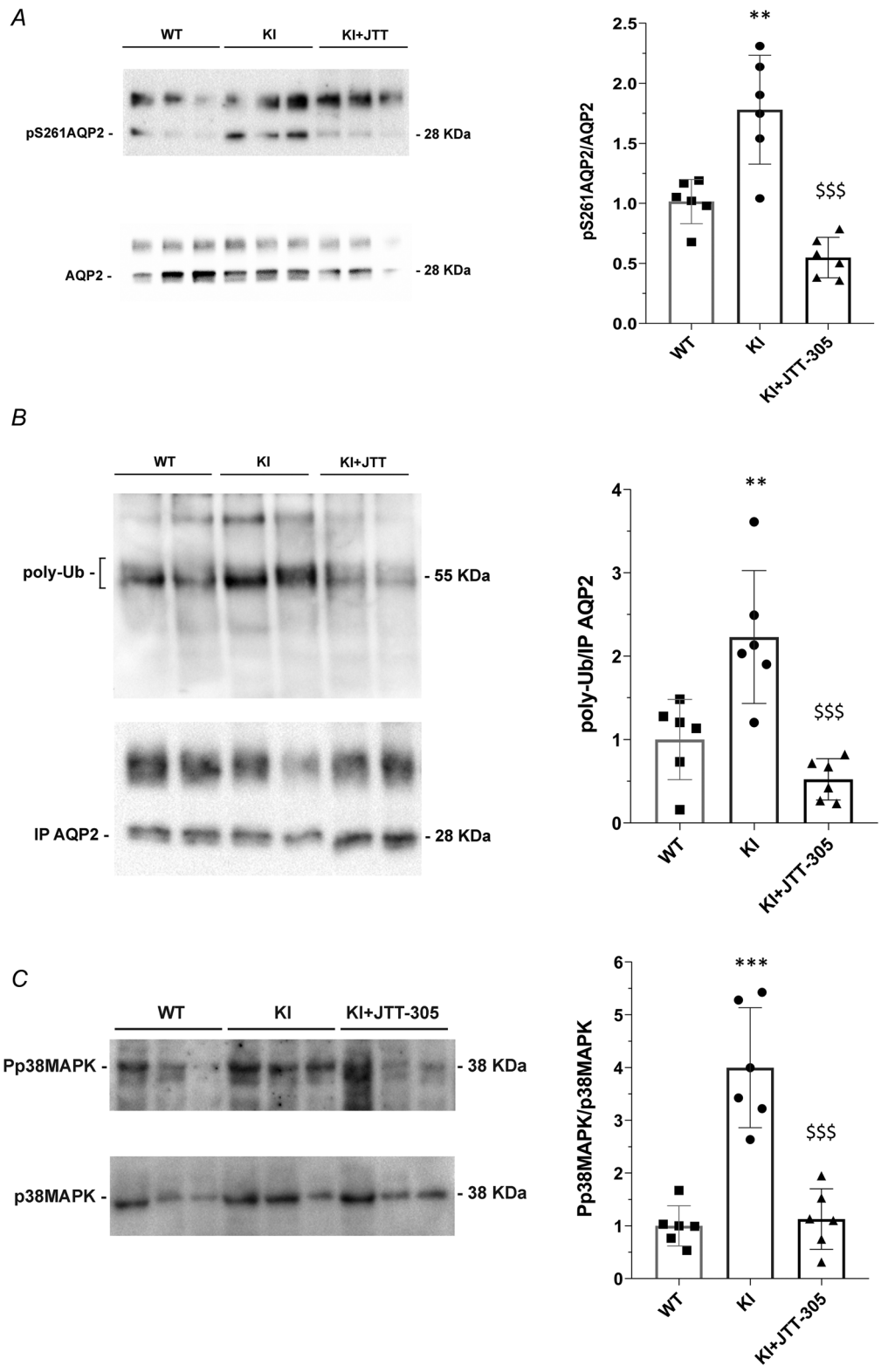

Figure 3. AQP2 phosphorylation at Ser261, ubiquitination and p38MAPK expression in the kidneys from WT, KI and JTT-305 treated KI mice
A, kidney slices from WT, KI and KI mice treated with JTT-305 were lysed and immunoblotting experiments were performed using specific antibodies against AQP2-pS261 and total AQP2. Densitometric analysis of AQP2-pS261 bands normalized to total AQP2 is reported in the histogram. Data are expressed as the mean ± SD (**$P = 0.0013$ *vs*. WT; $$$ $P = 0.00001$ *vs*. KI). *B*, kidney slices from WT, KI and KI mice treated with JTT-305 were lysed

© 2024 The Authors. *The Journal of Physiology* © 2024 The Physiological Society.

14697793, 0, Downloaded from https://physoc.onlinelibrary.wiley.com/doi/10.1113/JP284233 by University Degli Studi Di Bari, Wiley Online Library on [27/02/2024]. See the Terms and Conditions (https://onlinelibrary.wiley.com/terms-and-conditions) on Wiley Online Library for rules of use; OA articles are governed by the applicable Creative Commons License

and subjected to immunoprecipitation (IP) with AQP2 antibody. Immunoprecipitates were immunoblotted using anti-AQP2 and anti-ubiquitin antibodies. Statistical analysis of data showed ubiquitinated AQP2 (poly-Ub-AQP2; polyubiquitinated) levels, normalized to immunoprecipitated AQP2 (**P = 0.004 *vs*. WT; $$$$P$ = 0.0002 *vs*. KI). *C*, kidney slices from WT, KI and KI mice treated with JTT-305 were lysed and immunoblotting experiments were performed using specific antibodies against phospho-p38MAPK (Pp38MAPK) and total p38MAPK. Densitometric analysis of Pp38MAPK bands, normalized to total p38MAPK, is reported in the histogram. Data are expressed as the mean ± SD (***P = 0.000005 *vs*. WT; $$$ P = 0.000009 *vs*. KI).

restored polyubiquitinated AQP2 levels detected in KI mice [KI+JTT-305: 0.523 (0.248) O.D.; $P = 0.0002$; $n = 6$ for each genotype] (Fig. 3*B*).

Next, we evaluated the phosphorylation level of p38MAPK because the phosphorylated form (Pp38MAPK) represents the activated form of p38MAPK. Moreover, p38MAPK is a candidate kinase to phosphorylate AQP2 at Ser261 (Hoffert et al., 2006; Nedvetsky et al., 2010) and its phosphorylation represents a hallmark for ubiquitination and protein degradation via proteasome (Isobe et al., 2017; Nedvetsky et al., 2010). Statistical analysis of the data obtained from western blot experiments revealed that Pp38MAPK levels were ∼4-fold higher in KI mice compared to WT mice [KI: 3.998 (1.138) *vs*. WT: 1.000 (0.381) O.D.; $P = 0.000005$; $n = 6$ for each genotype] (Fig. 3*C*). Interestingly, KI mice treated with JTT-305 showed phosphorylation levels of p38MAPK no different from that observed in WT mice and significantly lower compared to KI mice [KI+JTT-305: 1.127 (0.573) O.D.; $P = 0.000009$; $n = 6$ for each genotype] (Fig. 3*C*).

CaSR overexpression downregulates AQP2 via miR137

We recently demonstrated the regulation of total AQP2 expression elicited by CaSR signalling via microRNA pathway activation (Ranieri et al., 2018). Showing a bimodal downregulation, p38MAPK on one side increases AQP2-pS261 levels, ubiquitination and degradation and, on the other side, increases miR137, a known AQP2-targeting miRNA in the kidney collecting duct (Kim et al., 2015; Ranieri et al., 2018).

Here, we evaluated the miR137 levels in KI mice kidneys compared to WT [KI: 6.622×10^{-7} (5.885×10^{-7}) *vs*. WT: 1.384×10^{-7} (1.283×10^{-7}) ng; $P = 0.033$; $n = 6$ for each genotype] (Fig. 4*A*), revealing a significant increase in KI mice miR137 levels. Treatment with JTT-305 of KI mice caused a significantly strong reduction of miR137 with respect to vehicle-treated KI mice [KI+JTT-305: 3.738×10^{-8} (3.939×10^{-8}) ng; $P = 0.009$; $n = 6$ for each genotype] (Fig. 4*A*).

A group of substrates activated by p38MAPK comprise transcription factors. Many transcription factors, such as transcription factor 1 (ATF1), encompassing a broad range of action, have been shown to be phosphorylated and subsequently activated by p38MAPK (Tan et al., 1996).

RT-PCR experiments were performed to evaluate the gene expression of ATF1 in the different genotypes (WT, KI and KI+JTT-305 mice). Compared with WT, ATF1 gene expression levels were significantly higher in KI mice kidneys [KI: 1.719 (0.272) *vs*. WT: 1.000 (0.249); $P = 0.004$; $n = 6$ for each genotype] (Fig. 4*B*). Of note, in JTT-305 KI mice, the calcilytic treatment prevented this increase, showing ATF1 mRNA levels similar to those obtained in WT mice [KI+JTT-305: 0.944 (0.428); $P = 0.002$; $n = 6$ for each genotype] (Fig. 4*B*). Moreover, the protein content of ATF1 and its phosphorylated form at serine 63 (pS63ATF1) was evaluated in kidneys from WT, KI and KI mice treated with JTT-305 by performing immunoblot experiments. In KI mice kidneys, we observed increased levels of the phosphorylated form of ATF1 (pS63ATF1), normalized to total protein content and total ATF1 levels, with respect to WT mice kidneys [KI: 1.553 (0.525) *vs*. WT: 1.000 (0.257); $P = 0.029$; $n = 6$ for each genotype] (Fig. 4*C*). Again, treatment with the calcilytic JTT-305 in KI mice restored the phosphorylated levels of ATF1 observed in WT mice [KI+JTT-305: 0.980 (0.282); $P = 0.024$; $n = 6$ for each genotype] (Fig. 4*C*).

p38MAPK increases miR137 via ATF1

Around half of the p38MAPK substrates identified so far are transcription factors (Zarubin & Han, 2005). Therefore, it is evident that p38MAPK has a pivotal role in regulating gene expression at transcriptional level. To verify the specific activation of ATF1 by p38MAPK, we used a specific p38MAPK inhibitor, SB203580. For this purpose, we performed *ex vivo* kidney slice preparations from KI mice kidneys, left in basal conditions or treated with the p38MAPK inhibitor SB203580. At first, we evaluated ATF1 mRNA levels. RT-PCR experiments revealed that the inhibition of p38MAPK caused a significant decrease in ATF1 mRNA levels compared to untreated KI mice kidney slices [KI SB203580: 0.395 (0.178) *vs*. KI ctrl: 1.000 (0.311); $P = 0.016$; $n = 6$ for each genotype] (Fig. 5*A*). Immunoblotting experiments showed a significant decline also in the phosphorylation levels of ATF1 (pS63ATF1) [KI SB203580: 0.505 (0.203) *vs*. KI ctrl: 1.000 (0.277) O.D.; $P = 0.005$; $n = 6$ for each genotype] (Fig. 5*B*). Next, we investigated the effect of the inhibition of p38MAPK on the high levels of miR137 observed in KI mice kidneys. KI SB203580 kidneys reported a robust decrease in miR137 levels compared

© 2024 The Authors. *The Journal of Physiology* © 2024 The Physiological Society.

14697793, 0, Downloaded from https://physoc.onlinelibrary.wiley.com/doi/10.1113/JP284233 by University Degli Studi Di Bari, Wiley Online Library on [27/02/2024]. See the Terms and Conditions (https://onlinelibrary.wiley.com/terms-and-conditions) on Wiley Online Library for rules of use; OA articles are governed by the applicable Creative Commons License

to KI untreated kidneys [KI SB203580: 1.207 × 10^{-6} (1.204 × 10^{-6}) *vs*. KI ctrl: 3.028 × 10^{-6} (2.255 × 10^{-6}) ng; $P = 0.047$; $n = 6$ for each genotype] (Fig. 5*C*). Moreover, the increase in total AQP2 levels, detected in KI mice kidneys, was prevented when treating KI mice kidney slices with p38MAPK inhibitor [KI SB203580: 1.605 (0.397) *vs*. KI ctrl: 1.000 (0.294) O.D.; $P = 0.029$; $n = 6$ for each genotype] (Fig. 5*D*). The inhibitory effect of SB203580 on p38MAPK phosphorylation was confirmed by immunoblotting experiments performed in KI mice kidney slices. As expected, Pp38MAPK levels decreased when KI mice kidney slices were treated with the inhibitor SB203580 [KI SB203580: 0.582 (0.236) *vs*. KI ctrl: 1.000 (0.315) O.D.; $P = 0.009$; $n = 6$ for each genotype] (Fig. 5*E*).

As stated in the methods section, three genotype mice (WT, KI and KI+JTT-305), three males and three females for each genotype, were used for all described experiments. No difference between the sexes were

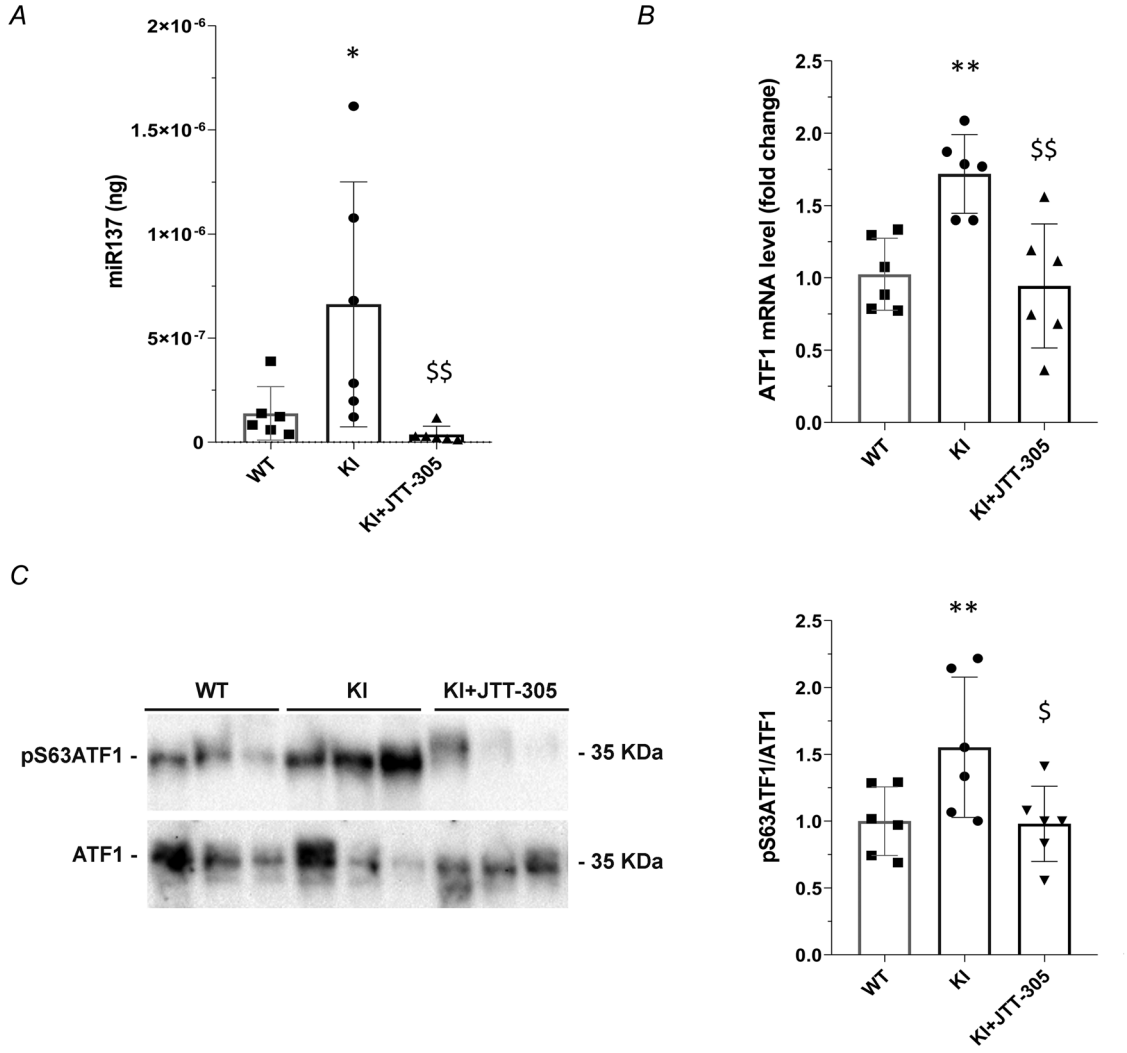

Figure 4. miR137 evaluation and ATF1 transcription factor expression in the kidneys from WT, KI and JTT-305 treated KI mice
A, total RNA was extracted from WT, KI and JTT-305 treated KI mice kidneys, and the cDNA was obtained as described in the Methods. Synthetic RNA with 59-phospho, miR137 (UUAUUGCUUAAGAAUACGCGUAG), was synthesized and used to perform a calibration curve and interpolate miRNA sample values from WT, KI and JTT-305 treated KI mice, to obtain a precise evaluation (in nanograms) of miR137 content in samples. Data from RT-PCR experiments were interpolated in the calibration curve obtained with synthetic miRNA. Data are expressed as the mean ± SD (*$P = 0.033$ *vs*. WT; $$P = 0.009$ *vs*. KI). *B*, for the analysis of ATF1 mRNA levels, RNA was extracted from WT, KI and JTT-305 treated KI mice kidneys as described in the Methods. Data are expressed as the mean ± SD (**$P = 0.004$ *vs*. WT; $$P = 0.002$ *vs*. KI). *C*, kidney slices from WT, KI and KI mice treated with JTT-305 were lysed and immunoblotting experiments were performed using specific antibodies against ATF1-pS63 and total ATF1. Densitometric analysis of ATF1-pS63bands normalized to total ATF1 is reported in the histogram. Data are expressed as the mean ± SD (*$P = 0.029$ *vs*. WT; $P = 0.024$ *vs*. KI).

© 2024 The Authors. *The Journal of Physiology* © 2024 The Physiological Society.

14697793, 0, Downloaded from https://physoc.onlinelibrary.wiley.com/doi/10.1113/JP284233 by University Degli Studi Di Bari, Wiley Online Library on [27/02/2024]. See the Terms and Conditions (https://onlinelibrary.wiley.com/terms-and-conditions) on Wiley Online Library for rules of use; OA articles are governed by the applicable Creative Commons License

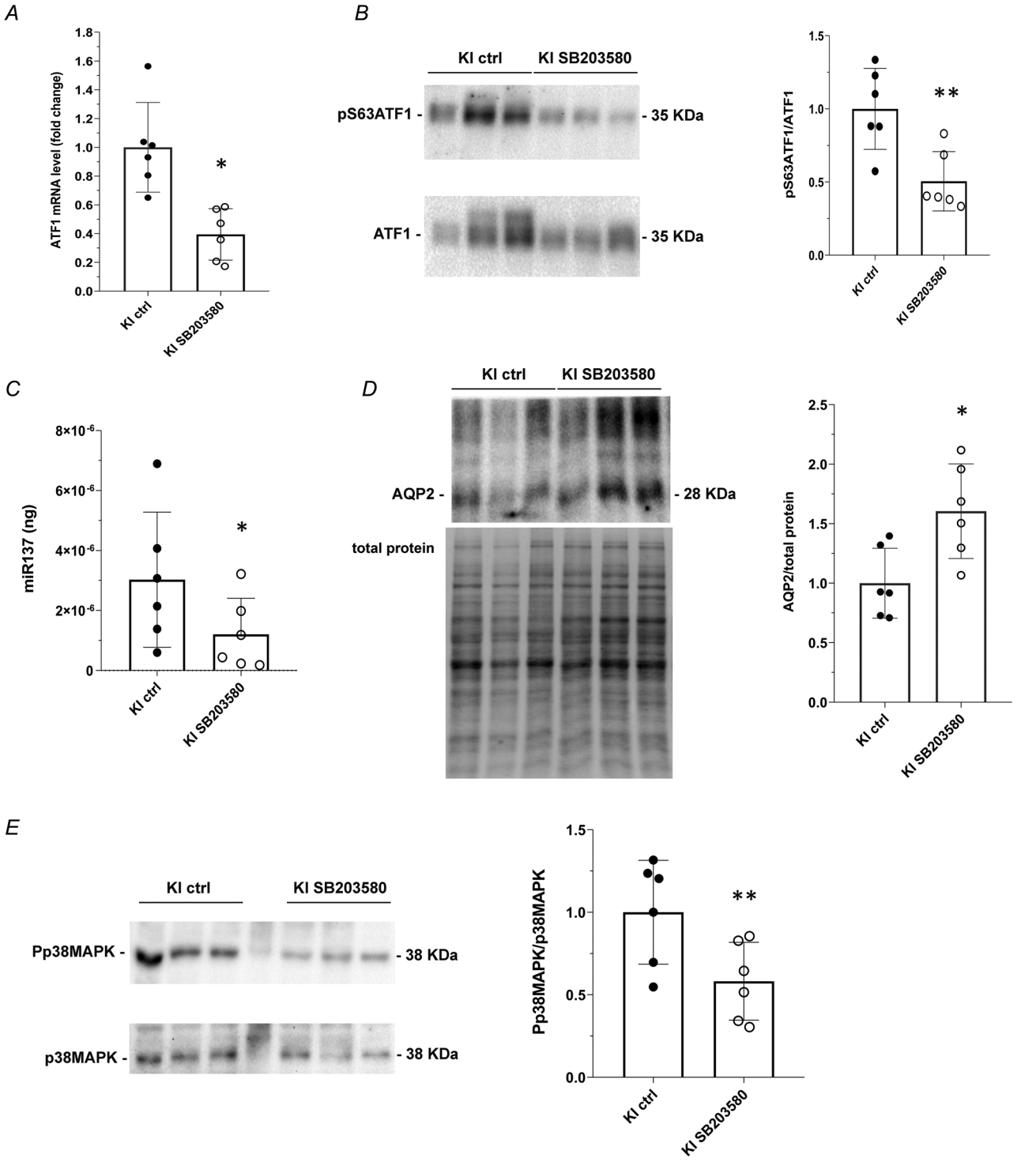

Figure 5. Modulation of ATF1, miR137 and AQP2 in response to p38MAPK inhibitor
A, for the analysis of ATF1 mRNA levels, RNA was extracted from KI kidney slices treated with p38MAPK inhibitor, SB203580, or left in basal conditions, as described in the Methods. Data are expressed as the mean ± SD (**P* = 0.016 *vs*. KI). *B*, kidney slices from KI ctrl and KI treated with SB203580 were lysed and immunoblotting experiments were performed using specific antibodies against ATF1-pS63 and total ATF1. Densitometric analysis of ATF1-pS63 bands normalized to total ATF1 is reported in the histogram. Data are expressed as the mean ± SD (***P* = 0.005 *vs*. KI). *C*, total RNA was extracted from KI ctrl and KI treated with SB203580 kidney slices, and the miRNA cDNA Synthesis Kit was used to obtain cDNA synthesis, as described in the Methods. Data from RT-PCR experiments were interpolated in the calibration curve obtained with synthetic miRNA. Data are expressed as the

© 2024 The Authors. *The Journal of Physiology* © 2024 The Physiological Society.

14697793, 0, Downloaded from https://physoc.onlinelibrary.wiley.com/doi/10.1113/JP284233 by University Degli Studi Di Bari, Wiley Online Library on [27/02/2024]. See the Terms and Conditions (https://onlinelibrary.wiley.com/terms-and-conditions) on Wiley Online Library for rules of use; OA articles are governed by the applicable Creative Commons License

mean ± SD (*P = 0.047 *vs.* KI). *D*, kidney slices from KI mice and KI mice treated with SB203580 were lysed and immunoblotting experiments were performed using specific antibodies against total AQP2. Densitometric analysis of total AQP2 bands normalized to the total protein content is reported in the histogram. Data are expressed as the mean ± SD (*P = 0.029 *vs.* KI). *E*, kidney slices from KI ctrl and KI treated with SB203580 were lysed and immunoblotting experiments were performed using specific antibodies against phospho-p38MAPK (Pp38MAPK) and total p38MAPK. Densitometric analysis of Pp38MAPK bands normalized to total p38MAPK is reported in the histogram. Data are expressed as the mean ± SD (**P = 0.009 *vs.* KI).

observed, indicating that the obtained results were not influenced by sex.

Discussion

The major result of the present study is the demonstration of *in vivo* treatment with calcilytic JTT-305/MK-5442 reversing the downregulation of the expression of the vasopressin-sensitive AQP2 water channel, resulting in an amelioration of the renal phenotype in CaSR KI mice mimicking ADH (Fig. 6).

Although we have provided evidence that high concentrations of urinary calcium counteract vasopressin action via the activation of the CaSR expressed at the luminal membrane of collecting duct cells, impairing the trafficking and the expression of AQP2, the present contribution provides a direct demonstration of this functional interplay. Specifically, the present study, as

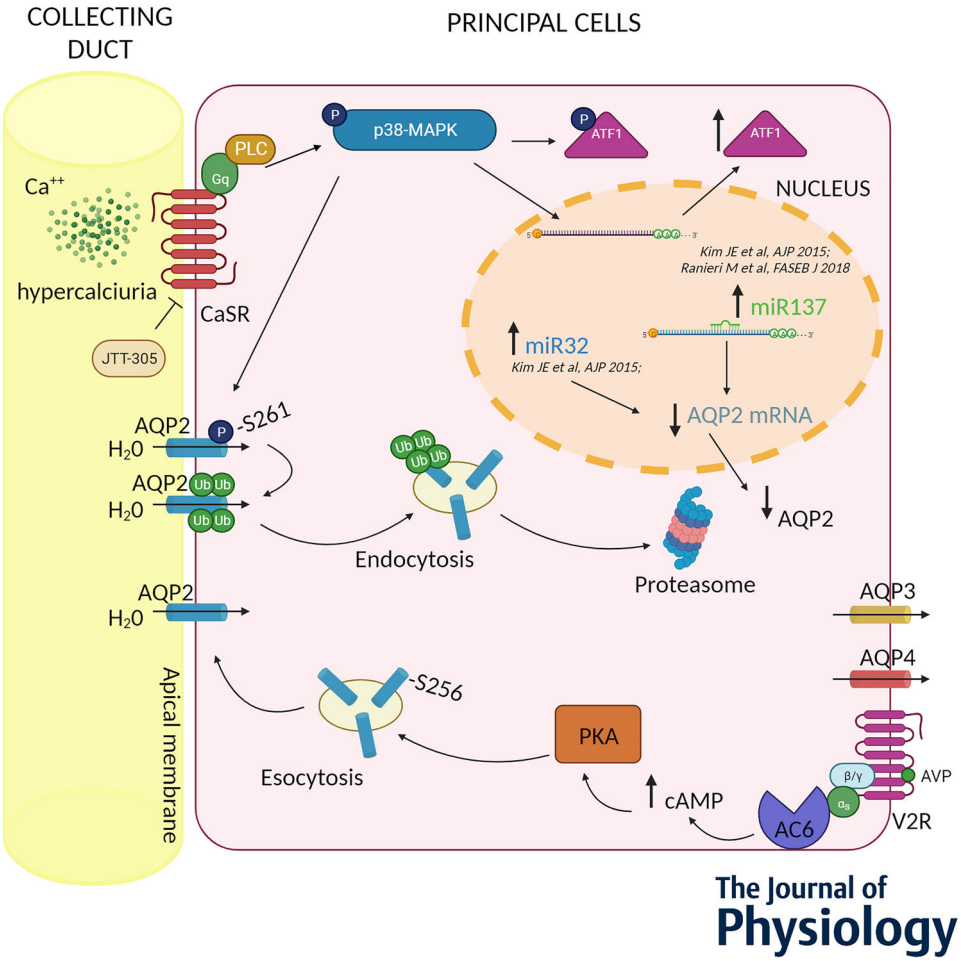

Figure 6. Schematic model
The proposed model shows that high urinary calcium levels in the collecting duct activate CaSR, resulting in the phosphorylation and activation of p38-MAPK that, in turn, phosphorylates AQP2 at Ser261, causing AQP2 internalization, ubiquitination (Ub) and proteasomal degradation. In parallel, CaSR signalling promotes the synthesis of miRNA137 via the activation of p38MAPK-ATF1, which results in reduced AQP2 mRNA translation (Ranieri et al., 2018). As reported by Kim et al. (2015), miRNA32 is also able to reduce AQP2 mRNA levels and consequently AQP2 abundance. The CaSR inhibition through calcilytic JTT-305 reverses the entire pathway.

© 2024 The Authors. *The Journal of Physiology* © 2024 The Physiological Society.

14697793, 0, Downloaded from https://physoc.onlinelibrary.wiley.com/doi/10.1113/JP284233 by University Degli Studi Di Bari, Wiley Online Library on [27/02/2024]. See the Terms and Conditions (https://onlinelibrary.wiley.com/terms-and-conditions) on Wiley Online Library for rules of use; OA articles are governed by the applicable Creative Commons License

performed on a mouse-based genetic model of CaSR KI, confirms that a constitutively active CaSR variant causes the downregulation of AQP2 expression via p38-MAPK-dependent increased AQP2-pS261 and AQP2 ubiquitination, leading to AQP2 protein degradation, as well as via the AQP2-targeting miR137 pathway. This interplay contributes to the impaired renal function and reduced renal concentrating ability that characterizes ADH.

It is well known that ADH patients develop hypocalcaemia, hyperphosphatemia and hypercalciuria and the current therapy is the administration of active vitamin D3 or PTH. However, this treatment aggravates hypercalciuria and renal calcification (Roszko, Hu et al., 2022). Interestingly, we have previously reported that treatment of CaSR KI mice with calcilytic JTT-305/MK-5442 increased urinary cAMP excretion, improved serum and urinary calcium and phosphate levels by stimulating endogenous PTH secretion, and prevented renal calcification (Dong et al., 2015). By contrast, PTH treatment normalized serum calcium and phosphate but could not reduce hypercalciuria or renal calcification (Dong et al., 2015). Because of this, calcilytics may become a treatment of choice for ADH patients. In the kidney, PTH stimulates calcium reabsorption in the distal convoluted tubule by activation of the calcium channel transient receptor potential vanilloid member 5 (i.e. TRPV5) (de Groot et al., 2008). This would allow for removal of calcium from the pro-urine without affecting sodium reabsorption, thus minimizing renal calcium wasting. However, its action probably does not prevent the hypercalciuric effect of activating mutations of the CASR gene. Conversely, JTT-305/MK-5442 reversed most of the ADH phenotypes of the CaSR KI mice, including a reduction in renal calcification. Calcilytics bind to the transmembrane domain of CaSR directly (Petrel et al., 2004) and allosterically stimulate the endogenous PTH release (Kumar et al., 2010).

The beneficial effect of JTT-305/MK-5442 on hypercalciuria and renal calcification is probably not restricted to an increased serum PTH level mimicking the effect of PTH. In the TAL CaSR is expressed on the basolateral membrane (Toka et al., 2015) and its main role is to inhibit calcium reabsorption in a PTH-independent fashion. This effect is accounted for, at least in part, by an increase in the paracellular pathway, as indicated by the concomitant downregulation of claudin-14 and of NKCC2 activation. Gong et al. (2015) have demonstrated that claudin-14 in the TAL is downstream of CaSR activation.

Specifically, CaSR controls the transcription of miR9 and miR-374 that target the 3′-untranslated region of the claudin-14 gene resulting in decreased paracellular divalent cation permeability contributing to pathological hypercalciuria and nephrocalcinosis. Thus, calcilytic drugs would be expected to decrease urinary calcium output via PTH-dependent and PTH-independent (renal CaSR-mediated) actions, hence potentially decreasing the risk of calcium stone occurrence.

CaSR activation in the TAL also decreases vasopressin-stimulated intracellular cAMP accumulation by inhibiting AC6 (de Jesus Ferreira et al., 1998). Therefore, we can speculate that the calcilytic JTT-305/MK-5442 can reverse most of the phenotypes of mutant CaSR KI mice and normalize not only serum calcium and phosphate, but also urinary calcium excretion, thus preventing renal calcification also in a PTH-independent action through vasopressin-dependent inhibition of cAMP synthesis in the TAL. This results in NKCC2 inhibition being necessary for paracellular calcium permeability. Calcium reabsorption in the TAL is reliant upon the uptake of NaCl across the luminal NKCC2 expressed on the luminal membrane. Potassium ions brought into the cell by NKCC2 are recycled back into the lumen through an apical K^+ channel. Together, these processes establish a lumen-positive transepithelial potential difference, which provides the driving force for the passive reabsorption of monovalent and divalent cations (Na^+, Ca^+ and Mg^{2+} ions) via the paracellular route. By attenuating the tonic inhibition of the vasopressin response in TAL as a result of the gain-of-function CaSR variant, the calcilytics reduce calcium wasting in the lumen preventing hypercalciuria and renal calcification.

In the collecting duct, we have previously provided evidence that high concentrations of luminal calcium counteract vasopressin action, thereby impairing the trafficking of the vasopressin-sensitive water channel, AQP2. This effect is mediated by the activation of the CaSR (Procino et al., 2004, 2008; Ranieri et al., 2015). Data that support this conclusion were obtained both from *in vitro* experiments conducted in renal collecting duct cells (Ranieri et al., 2015) and from hypercalciuric patients (Procino et al., 2012), as well as from bed rest studies (Tamma, Di Mise et al., 2014). Moreover, high external calcium has been found to reduce AQP2 expression, in both collecting duct cell lines and hypercalciuric rats (Bustamante et al., 2008; Procino et al., 2004; Sands et al., 1998). Specifically, CaSR activation in renal cells has been demonstrated to modulate AQP2 trafficking and/or expression by altering its phosphorylation state (Ranieri et al., 2013, 2015), which indicates a direct negative effect on the vasopressin-sensitive water channel, AQP2. Finally, in pendrin/NaCl cotransporter double-knockout mice with significant calcium wasting and developing severe volume depletion despite increased circulating vasopressin levels, we have demonstrated that CaSR-mediated impairment of AQP2 expression/trafficking underlies vasopressin resistance observed in double-knockout mice (Ranieri, 2019; Ranieri et al., 2018).

To conclude, our data show that CaSR KI mice mimicking ADH are characterized by downregulation

© 2024 The Authors. *The Journal of Physiology* © 2024 The Physiological Society.

14697793, 0, Downloaded from https://physoc.onlinelibrary.wiley.com/doi/10.1113/JP284233 by University Degli Studi Di Bari, Wiley Online Library on [27/02/2024]. See the Terms and Conditions (https://onlinelibrary.wiley.com/terms-and-conditions) on Wiley Online Library for rules of use; OA articles are governed by the applicable Creative Commons License

of AQP2 expression associated with CaSR-dependent activation of AQP2 degradation and reduced expression via AQP2-targeting miRNA137. Of note, the inhibition of constitutively active CaSR by *in vivo* treatment with calcilytics restores normal levels of AQP2 expression, providing direct *in vivo* evidence for a critical role of CaSR in the negative regulation of vasopressin-AQP2-dependent water reabsorption in the collecting duct. The amelioration of most of the abnormalities in calcium metabolism including hypercalciuria, renal calcification and AQP2-mediated osmotic water reabsorption makes calcilytic a good candidate for a novel therapeutic agent in the treatment of ADH.

References

Alfadda, T. I., Saleh, A. M. A., Houillier, P., & Geibel, J. P. (2014). Calcium-sensing receptor 20 years later. *American Journal of Physiology-Cell Physiology*, **307**(3), C221–C231.

Ba, J., Brown, D., & Friedman, P. A. (2003). Calcium-sensing receptor regulation of PTH-inhibitable proximal tubule phosphate transport. *American Journal of Physiology-Renal Physiology*, **285**(6), F1233–F1243.

Brown, E. M., & Macleod, R. J. (2001). Extracellular calcium sensing and extracellular calcium signaling. *Physiological Reviews*, **81**(1), 239–297.

Bustamante, M., Hasler, U., Leroy, V. C. A. A. R., De Seigneux, S., Dimitrov, M., Mordasini, D., Rousselot, M., Martin, P.-Y., & Féraille, E. (2008). Calcium-sensing receptor attenuates AVP-induced aquaporin-2 expression via a calmodulin-dependent mechanism. *Journal of the American Society of Nephrology: JASN*, **19**(1), 109–116.

Centrone, M., Ranieri, M., Di Mise, A. D. i., Berlingerio, S. P., Russo, A., Deen, P. M. T., Staub, O., Valenti, G., & Tamma, G. (2017). AQP2 abundance is regulated by the E3-ligase CHIP Via HSP70. *Cellular Physiology and Biochemistry: International Journal of Experimental Cellular Physiology, Biochemistry, and Pharmacology*, **44**(2), 515–531.

Chau, V., Tobias, J. W., Bachmair, A., Marriott, D., Ecker, D. J., Gonda, D. K., & Varshavsky, A. (1989). A multiubiquitin chain is confined to specific lysine in a targeted short-lived protein. *Science (New York, NY)*, **243**(4898), 1576–1583.

De Groot, T., Bindels, R. J. M., & Hoenderop, J. G. J. (2008). TRPV5: an ingeniously controlled calcium channel. *Kidney International*, **74**(10), 1241–1246.

Dong, B., Endo, I., Ohnishi, Y., Kondo, T., Hasegawa, T., Amizuka, N., Kiyonari, H., Shioi, G.o, Abe, M., Fukumoto, S., & Matsumoto, T. (2015). Calcilytic ameliorates abnormalities of mutant calcium-sensing receptor (CaSR) knock-in mice mimicking autosomal dominant hypocalcemia (ADH). *Journal of Bone and Mineral Research: The Official Journal of the American Society for Bone and Mineral Research*, **30**(11), 1980–1993.

Ferreira, M. C. D. E. J., Héliès-Toussaint, C., Imbert-Teboul, M., Bailly, C., Verbavatz, J.-M., Bellanger, A.-C., & Chabardès, D. (1998). Co-expression of a Ca^{2+}-inhibitable adenylyl cyclase and of a Ca^{2+}-sensing receptor in the cortical thick ascending limb cell of the rat kidney. Inhibition of hormone-dependent cAMP accumulation by extracellular Ca^{2+}. *The Journal of Biological Chemistry*, **273**(24), 15192–15202.

Fenton, R. A., & Moeller, H. B. (2008). Recent discoveries in vasopressin-regulated aquaporin-2 trafficking. *Progress in Brain Research*, **170**, 571–579.

Finley, D., Sadis, S., Monia, B. P., Boucher, P., Ecker, D. J., Crooke, S. T., & Chau, V. (1994). Inhibition of proteolysis and cell cycle progression in a multiubiquitination-deficient yeast mutant. *Molecular and Cellular Biology*, **14**, 5501–5509.

Flick, K., Ouni, I., Wohlschlegel, J. A., Capati, C., Mcdonald, W. H., Yates, J. R., & Kaiser, P. (2004). Proteolysis-independent regulation of the transcription factor Met4 by a single Lys 48-linked ubiquitin chain. *Nature Cell Biology*, **6**(7), 634–641.

Gafni, R. I., Brahim, J. S., Andreopoulou, P., Bhattacharyya, N., Kelly, M. H., Brillante, B. A., Reynolds, J. C., Zhou, H., Dempster, D. W., & Collins, M. T. (2012). Daily parathyroid hormone 1–34 replacement therapy for hypoparathyroidism induces marked changes in bone turnover and structure. *Journal of Bone and Mineral Research: The Official Journal of the American Society for Bone and Mineral Research*, **27**(8), 1811–1820.

Gong, Y., Himmerkus, N., Plain, A., Bleich, M., & Hou, J. (2015). Epigenetic regulation of microRNAs controlling CLDN14 expression as a mechanism for renal calcium handling. *Journal of the American Society of Nephrology: JASN*, **26**(3), 663–676.

Hebert, S. C., Brown, E. M., & Harris, H. W. (1997). Role of the Ca(2+)-sensing receptor in divalent mineral ion homeostasis. *The Journal of Experimental Biology*, **200**(2), 295–302.

Hicke, L., & Dunn, R. (2003). Regulation of membrane protein transport by ubiquitin and ubiquitin-binding proteins. *Annual Review of Cell and Developmental Biology*, **19**(1), 141–172.

Hoffert, J. D., Fenton, R. A., Moeller, H. B., Simons, B., Tchapyjnikov, D., Mcdill, B. W., Yu, M.-J., Pisitkun, T., Chen, F., & Knepper, M. A. (2008). Vasopressin-stimulated increase in phosphorylation at Ser269 potentiates plasma membrane retention of aquaporin-2. *The Journal of Biological Chemistry*, **283**(36), 24617–24627.

Hoffert, J. D., Nielsen, J., Yu, M.-J., Pisitkun, T., Schleicher, S. M., Nielsen, S., & Knepper, M. A. (2007). Dynamics of aquaporin-2 serine-261 phosphorylation in response to short-term vasopressin treatment in collecting duct. *American Journal of Physiology-Renal Physiology*, **292**(2), F691–F700.

© 2024 The Authors. *The Journal of Physiology* © 2024 The Physiological Society.

14697793, 0, Downloaded from https://physoc.onlinelibrary.wiley.com/doi/10.1113/JP284233 by University Degli Studi Di Bari, Wiley Online Library on [27/02/2024]. See the Terms and Conditions (https://onlinelibrary.wiley.com/terms-and-conditions) on Wiley Online Library for rules of use; OA articles are governed by the applicable Creative Commons License

Hoffert, J. D., Pisitkun, T., Wang, G., Shen, R.-F., & Knepper, M. A. (2006). Quantitative phosphoproteomics of vasopressin-sensitive renal cells: regulation of aquaporin-2 phosphorylation at two sites. *Proceedings of the National Academy of Sciences of the United States of America*, **103**(18), 7159–7164.

Hough, T. A., Bogani, D., Cheeseman, M. T., Favor, J., Nesbit, M. A., Thakker, R. V., & Lyon, M. F. (2004). Activating calcium-sensing receptor mutation in the mouse is associated with cataracts and ectopic calcification. *The Proceedings of the National Academy of Sciences USA*, **101**(37), 13566–13571.

Isobe, K., Jung, H. J., Yang, C. R., Claxton, J., Sandoval, P., Burg, M. B., Raghuram, V., & Knepper, M. A. (2017). Systems-level identification of PKA-dependent signaling in epithelial cells. *Proceedings of the National Academy of Sciences of the United States of America*, **114**, E8875–E8884.

Kim, J.-E., Jung, H. J., Lee, Y.u-J., & Kwon, T.-H. (2015). Vasopressin-regulated miRNAs and AQP2-targeting miRNAs in kidney collecting duct cells. *American Journal of Physiology-Renal Physiology*, **308**(7), F749–F764.

Kimura, S., Nakagawa, T., Matsuo, Y., Ishida, Y., Okamoto, Y., & Hayashi, M. (2011). JTT-305, an orally active calcium-sensing receptor antagonist, stimulates transient parathyroid hormone release and bone formation in ovariectomized rats. *European Journal of Pharmacology*, **668**(1–2), 331–336.

Kumar, S., Matheny, C. J., Hoffman, S. J., Marquis, R. W., Schultz, M., Liang, X., Vasko, J. A., Stroup, G. B., Vaden, V. R., Haley, H., Fox, J., Delmar, E. G., Nemeth, E. F., Lago, A. M., Callahan, J. F., Bhatnagar, P., Huffman, W. F., Gowen, M., Yi, B., Danoff, T. M., & Fitzpatrick, L. A. (2010). An orally active calcium-sensing receptor antagonist that transiently increases plasma concentrations of PTH and stimulates bone formation. *Bone*, **46**(2), 534–542.

Li, W., & Ye, Y. (2008). Polyubiquitin chains: Functions, structures, and mechanisms. *Cellular and Molecular Life Sciences: CMLS*, **65**(15), 2397–2406.

Matsumura, Y., Uchida, S., Rai, T., Sasaki, S., & Marumo, F. (1997). Transcriptional regulation of aquaporin-2 water channel gene by cAMP. *Journal of the American Society of Nephrology: JASN*, **8**(6), 861–867.

Moeller, H. B., Olesen, E. T. B., & Fenton, R. A. (2011). Regulation of the water channel aquaporin-2 by posttranslational modification. *American Journal of Physiology-Renal Physiology*, **300**(5), F1062–F1073.

Nedvetsky, P. I., Tabor, V., Tamma, G., Beulshausen, S., Skroblin, P., Kirschner, A., Mutig, K., Boltzen, M., Petrucci, O., Vossenkämper, A., Wiesner, B., Bachmann, S., Rosenthal, W., & Klussmann, E. (2010). Reciprocal regulation of aquaporin-2 abundance and degradation by protein kinase A and p38-MAP kinase. *Journal of the American Society of Nephrology: JASN*, **21**(10), 1645–1656.

Nedvetsky, P. I., Tamma, G., Beulshausen, S., Valenti, G., Rosenthal, W., & Klussmann, E. (2009). Regulation of aquaporin-2 trafficking. *Handbook of Experimental Pharmacology*, **190**, 133–157.

Pearce, S.h, & Thakker, R.v (1997). The calcium-sensing receptor: Insights into extracellular calcium homeostasis in health and disease. *The Journal of Endocrinology*, **154**(3), 371–378.

Petrel, C., Kessler, A., Dauban, P., Dodd, R. H., Rognan, D., & Ruat, M. (2004). Positive and negative allosteric modulators of the Ca^{2+}-sensing receptor interact within overlapping but not identical binding sites in the transmembrane domain. *The Journal of Biological Chemistry*, **279**(18), 18990–18997.

Pollak, M. R., Brown, E. M., Chou, Y.-H. W.u, Hebert, S. C., Marx, S. J., Stelnmann, B., Levi, T., Seidman, C. E., & Seidman, J. G. (1993). Mutations in the human Ca(2+)-sensing receptor gene cause familial hypocalciuric hypercalcemia and neonatal severe hyperparathyroidism. *Cell*, **75**(7), 1297–1303.

Pollak, M. R., Brown, E. M., Estep, H. L., Mclaine, P. N., Kifor, O., Park, J.i, Hebert, S. C., Seidman, C. E., & Seidman, J. G. (1994). Autosomal dominant hypocalcaemia caused by a Ca(2+)-sensing receptor gene mutation. *Nature Genetics*, **8**(3), 303–307.

Procino, G., Carmosino, M., Tamma, G., Gouraud, S., Laera, A., Riccardi, D., Svelto, M., & Valenti, G. (2004). Extracellular calcium antagonizes forskolin-induced aquaporin 2 trafficking in collecting duct cells. *Kidney International*, **66**(6), 2245–2255.

Procino, G., Mastrofrancesco, L., Mira, A., Tamma, G., Carmosino, M., Emma, F., Svelto, M., & Valenti, G. (2008). Aquaporin 2 and apical calcium-sensing receptor: New players in polyuric disorders associated with hypercalciuria. *Seminars in Nephrology*, **28**(3), 297–305.

Procino, G., Mastrofrancesco, L., Tamma, G., Lasorsa, D. R., Ranieri, M., Stringini, G., Emma, F., Svelto, M., & Valenti, G. (2012). Calcium-sensing receptor and aquaporin 2 interplay in hypercalciuria-associated renal concentrating defect in humans. An in vivo and in vitro study. *PLoS One*, **7**(3), e33145.

Ranieri, M. (2019). Renal Ca(2+) and water handling in response to calcium sensing receptor signaling: physiopathological aspects and role of CaSR-regulated microRNAs. *International Journal of Molecular Sciences*, **20**(21), 5341.

Ranieri, M., Tamma, G., Di Mise, A., Russo, A., Centrone, M., Svelto, M., Calamita, G., & Valenti, G. (2015). Negative feedback from CaSR signaling to aquaporin-2 sensitizes vasopressin to extracellular Ca2. *Journal of Cell Science*, **128**(13), 2350–2360.

Ranieri, M., Tamma, G., Di Mise, A., Vezzoli, G., Soldati, L., Svelto, M., & Valenti, G. (2013). Excessive signal transduction of gain-of-function variants of the calcium-sensing receptor (CaSR) are associated with increased ER to cytosol calcium gradient. *PLoS One*, **8**(11), e79113.

Ranieri, M., Zahedi, K., Tamma, G., Centrone, M., Di Mise, A., Soleimani, M., & Valenti, G. (2018). CaSR signaling down-regulates AQP2 expression via a novel microRNA pathway in pendrin and NaCl cotransporter knockout mice. *FASEB Journal: Official Publication of the Federation of American Societies for Experimental Biology*, **32**(4), 2148–2159.

© 2024 The Authors. *The Journal of Physiology* © 2024 The Physiological Society.

14697793, 0, Downloaded from https://physoc.onlinelibrary.wiley.com/doi/10.1113/JP284233 by University Degli Studi Di Bari, Wiley Online Library on [27/02/2024]. See the Terms and Conditions (https://onlinelibrary.wiley.com/terms-and-conditions) on Wiley Online Library for rules of use; OA articles are governed by the applicable Creative Commons License

Riccardi, D., & Valenti, G. (2016). Localization and function of the renal calcium-sensing receptor. *Nature Reviews Nephrology*, **12**(7), 414–425.
Roszko, K. L., Hu, T. Y., Guthrie, L. C., Brillante, B. A., Smith, M., Collins, M. T., & Gafni, R. I. (2022). PTH 1–34 replacement therapy has minimal effect on quality of life in patients with hypoparathyroidism. *Journal of Bone and Mineral Research: The Official Journal of the American Society for Bone and Mineral Research*, **37**(1), 68–77.
Roszko, K. L., Stapleton Smith, L. M., Sridhar, A. V., Roberts, M. S., Hartley, I. R., Gafni, R. I., Collins, M. T., Fox, J. C., & Nemeth, E. F. (2022). Autosomal dominant hypocalcemia type 1: A systematic review. *Journal of Bone and Mineral Research: The Official Journal of the American Society for Bone and Mineral Research*, **37**(10), 1926–1935.
Sadowski, M., Suryadinata, R., Tan, A. R., Roesley, S. N. A., & Sarcevic, B. (2012). Protein monoubiquitination and polyubiquitination generate structural diversity to control distinct biological processes. *Iubmb Life*, **64**(2), 136–142.
Sands, J. M., Flores, F. X., Kato, A., Baum, M. A., Brown, E. M., Ward, D. T., Hebert, S. C., & Harris, H. W. (1998). Vasopressin-elicited water and urea permeabilities are altered in IMCD in hypercalcemic rats. *The American Journal of Physiology*, **274**, F978–F985.
Sands, J. M., Naruse, M., Baum, M., Jo, I., Hebert, S. C., Brown, E. M., & Harris, H. W. (1997). Apical extracellular calcium/polyvalent cation-sensing receptor regulates vasopressin-elicited water permeability in rat kidney inner medullary collecting duct. *The Journal of Clinical Investigation*, **99**(6), 1399–1405.
Sikjaer, T., Rejnmark, L., Rolighed, L., Heickendorff, L., & Mosekilde, L. (2011). The effect of adding PTH(1–84) to conventional treatment of hypoparathyroidism: A randomized, placebo-controlled study. *Journal of Bone and Mineral Research: The Official Journal of the American Society for Bone and Mineral Research*, **26**(10), 2358–2370.
Tamma, G., Di Mise, A., Ranieri, M., Svelto, M., Pisot, R., Bilancio, G., Cavallo, P., De Santo, N. G., Cirillo, M., & Valenti, G. (2014). A decrease in aquaporin 2 excretion is associated with bed rest induced high calciuria. *Journal of translational medicine*, **12**(1), 133.
Tamma, G., Ranieri, M., Di Mise, A., Centrone, M., Svelto, M., & Valenti, G. (2014). Glutathionylation of the aquaporin-2 water channel: A novel post-translational modification modulated by the oxidative stress. *The Journal of Biological Chemistry*, **289**(40), 27807–27813.
Tan, Y., Rouse, J., Zhang, A., Cariati, S., Cohen, P., & Comb, M. J. (1996). FGF and stress regulate CREB and ATF-1 via a pathway involving p38 MAP kinase and MAPKAP kinase-2. *The EMBO Journal*, **15**(17), 4629–4642.
Theman, T. A., Collins, M. T., Dempster, D. W., Zhou, H., Reynolds, J. C., Brahim, J. S., Roschger, P., Klaushofer, K., & Winer, K. K. (2009). PTH(1–34) replacement therapy in a child with hypoparathyroidism caused by a sporadic calcium receptor mutation. *Journal of Bone and Mineral Research: The Official Journal of the American Society for Bone and Mineral Research*, **24**(5), 964–973.
Thrower, J. S. (2000). Recognition of the polyubiquitin proteolytic signal. *The EMBO Journal*, **19**(1), 94–102.
Toka, H. R., Pollak, M. R., & Houillier, P. (2015). Calcium sensing in the renal tubule. *Physiology (Bethesda, Md)*, **30**, 317–326.
Trepiccione, F., Pisitkun, T., Hoffert, J. D., Poulsen, S. B., Capasso, G., Nielsen, S., Knepper, M. A., Fenton, R. A., & Christensen, B. M. (2014). Early targets of lithium in rat kidney inner medullary collecting duct include p38 and ERK1/2. *Kidney International*, **86**(4), 757–767.
Vezzoli, G., Terranegra, A., Rainone, F., Arcidiacono, T., Cozzolino, M., Aloia, A., Dogliotti, E., Cusi, D., & Soldati, L. (2011). Calcium-sensing receptor and calcium kidney stones. *Journal of Translational Medicine*, **9**(1), 201.
Ward, D., & Riccardi, D. (2002). Renal physiology of the extracellular calcium-sensing receptor. *Pflugers Archiv: European Journal of Physiology*, **445**(2), 169–176.
Zarubin, T., & Han, J. (2005). Activation and signaling of the p38 MAP kinase pathway. *Cell Research*, **15**(1), 11–18.

Additional information

Data availability statement

All data supporting the results are provided within the paper itself. The statistical summary document contains data that support the findings of the present study.

Competing interests

The authors declare that they have no competing interests.

Author contributions

The experiments were performed in the following laboratories: Laboratory of Cell Physiology, Department of Biosciences, Biotechnologies and Environment, University of Bari, Bari, Italy; Laboratory in the Department of Bioregulatory Sciences, Tokushima University, Tokushima, Japan. MR, IE, SF, TM and GV designed and performed the experiments and analysed the data. M.R., I.A., M.D., A.F., M.V., A.D.M., M.C., M.M., G.T. and G.V. interpretated the data, wrote the manuscript and read the manuscript critically. All authors approved the final version of the manuscript submitted for publication and agree to be accountable for all aspects of the work in ensuring that questions related to the accuracy or integrity of any part of the work are appropriately investigated and resolved. All persons designated as authors qualify for authorship, and all those who qualify for authorship are listed.

Funding

MR is supported financially by 'POR Puglia FESR FSE 2014—2020 – Asse X – Azione 10.4. – Atto Dirigenziale 162/DIR/2019/00057 del 13/05/2019: Avviso pubblico n. 2/FSE/2019 'Research for Innovation' (REFIN) – (code 4FC8E072). ADM is supported by 'Attrazione e Mobilità

© 2024 The Authors. *The Journal of Physiology* © 2024 The Physiological Society.

14697793, 0, Downloaded from https://physoc.onlinelibrary.wiley.com/doi/10.1113/JP284233 by University Degli Studi Di Bari, Wiley Online Library on [27/02/2024]. See the Terms and Conditions (https://onlinelibrary.wiley.com/terms-and-conditions) on Wiley Online Library for rules of use; OA articles are governed by the applicable Creative Commons License

dei Ricercatori, PON 'R&I' 2014−2020, Azione I.2' (code AIM1893457-3, linea 1).

Keywords

AQP2, autosomal dominant hypocalcaemia, calcilytic, CaSR, microRNA, vasopressin, vasopressin type 2 receptor

Supporting information

Additional supporting information can be found online in the Supporting Information section at the end of the HTML view of the article. Supporting information files available:

Peer Review History

© 2024 The Authors. *The Journal of Physiology* © 2024 The Physiological Society.

14697793, 0, Downloaded from https://physoc.onlinelibrary.wiley.com/doi/10.1113/JP284233 by University Degli Studi Di Bari, Wiley Online Library on [27/02/2024]. See the Terms and Conditions (https://onlinelibrary.wiley.com/terms-and-conditions) on Wiley Online Library for rules of use; OA articles are governed by the applicable Creative Commons License